

# Modeling electromagnetic field excitation and rf power absorption in a large helicon plasma

Konstantin P. Shamrai<sup>a</sup>, Shunjiro Shinohara<sup>b,\*</sup>

<sup>a</sup> Institute for Nuclear Research, National Academy of Sciences, 03680 Kiev, Ukraine

<sup>b</sup> Interdisciplinary Graduate School of Engineering Sciences, Kyushu University, Kasuga, Fukuoka 816-8580, Japan

Available online 21 November 2005

## Abstract

Wave propagation and rf power absorption are considered in a large helicon plasma source excited by a flat antenna along the magnetic field. Various single-, four- and six-turn antennas of different dimensions are examined comparatively. The simple physical model and computation code accounting for the most important features of the system are introduced. Profiles of the rf magnetic field and absorbed power and the antenna loading resistance are computed over a broad range of parameters. Computation results are interpreted considering propagation characteristics of the waves, such as the group velocity and characteristic angle, and are compared with measured data.

© 2005 Elsevier B.V. All rights reserved.

**Keywords:** Helicon plasma; Inductively coupled magnetized plasma; Rf field; Radiation resistance; Group velocity

## 1. Introduction

Helicon sources can produce dense plasmas over a broad range of operating parameters [1,2] and, therefore, are attractive for various applications including thin film deposition (e.g., [2–5] and references therein). These devices are known in two different basic configurations. The first is a conventional helicon plasma with a shell antenna enveloping the dielectric discharge chamber and launching the rf power across the magnetic field [1,2]. The second is magnetically enhanced inductively coupled plasma (or inductively coupled magnetized plasma, ICMP) with a planar antenna located behind the dielectric window and launching the power along the magnetic field [6–9]. Latter devices provide a unique possibility for generating plasmas of densities above  $10^{12}$  cm<sup>-3</sup> in the large chambers, e.g., 45-cm diameter and 170-cm long [7,8], and 75-cm diameter and 486-cm long [9], with moderate power in the range of 100 W. So extensive the

plasmas are promising for basic research, such as modeling of space relevant phenomena, and for applications, such as processing of large surfaces, decomposition of hazardous materials and space propulsion.

Various models have been developed for characterizing the ICMPs. TASK/WF code which assumes a cold plasma of fixed profile [10] is especially effective for computations with complicated, e.g., cusped magnetic fields [11,12]. Another model accounts for kinetic effects but neglects the plasma and magnetic field nonuniformity and the radial structure of the rf fields [13]. The most complete model considers both electromagnetic and discharge effects [14]; however, it needs so much computation time that normally compels one to ignore small-scale rf electrostatic effects.

We present a simple model that is convenient for quick computation of the rf fields, power deposition and antenna loading resistance in the large ICMPs. It assumes a cold plasma with prescribed (either radially or axially nonuniform) density profile and takes the radial field structure into account. Computation results for different large ICMPs excited by various single- and multi-turn antennas are interpreted considering wave

\* Corresponding author. Tel.: +81 92 5837649; fax: +81 92 5718894.

E-mail addresses: [kshamrai@kinr.kiev.ua](mailto:kshamrai@kinr.kiev.ua) (K.P. Shamrai), [shinohara@aces.kyushu-u.ac.jp](mailto:shinohara@aces.kyushu-u.ac.jp) (S. Shinohara).

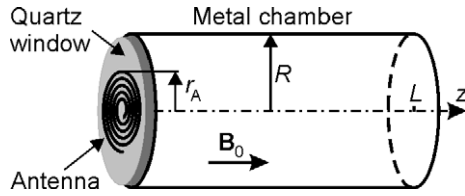


Fig. 1. A scheme of the inductively coupled magnetized plasma (ICMP).

propagation characteristics and compared with the experimental data.

## 2. Theoretical model and computation results

The ICMP is assumed as a cylindrical metal chamber of radius  $R$  and length  $L$  terminated, at one end, by a metal plate and by a quartz window of width  $d$ , at the other end (Fig. 1). A planar antenna is located on the outer surface of the window and consists of  $N$  thin rings of radii  $r_{An} = r_A(n/N)$  ( $n=1, \dots, N$ ) where  $r_A$  is the total antenna radius. Each of the rings contains the rf currents  $I_A \cos \omega t$ . Plasma density is supposed to be either uniform, or axially nonuniform,  $n = n_0(z)$ , or radially nonuniform,  $n = n_0(r)$ . A uniform magnetic field  $B_0$  is applied along the  $z$ -axis.

The rf fields are described by Maxwell equations with cold-plasma permittivity tensor and the antenna current density represented as  $\mathbf{j}_A = \hat{\mathbf{e}}_\theta I_A \delta(z+d) \sum_{n=1}^N \delta(r - r_{An}) \cos \omega t$ . Using Fourier-Bessel series, e.g.,

$$\begin{pmatrix} E_r \\ E_\theta \\ E_z \end{pmatrix} = \sum_{i=1}^{\infty} \begin{pmatrix} F_{ri}(z) J_1(k_{\perp i} r) \\ F_{\theta i}(z) J_1(k_{\perp i} r) \\ F_{zi}(z) J_0(k_{\perp i} r) \end{pmatrix} e^{-i\omega t} + cc, \quad (1)$$

where  $J_{0,1}$  are the Bessel functions and  $k_{\perp i} = \lambda_i/R$  are (discrete) perpendicular wave numbers with  $\lambda_i$  being the  $i$ th root of  $J_1$ , reduces the Maxwell equations to the set of ordinary differential equations for the amplitudes  $F$ . These equations are solved with appropriate boundary conditions on interfaces, and the solutions are used to combine the total fields, Eq. (1). Results presented in this section were computed for the Ar plasma with

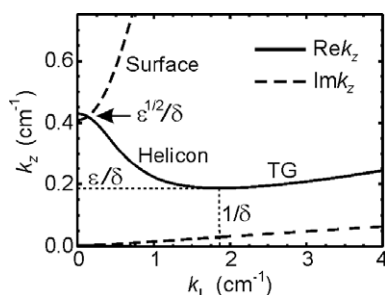


Fig. 2. Wave dispersion curves computed for the parameters of Eq. (2).

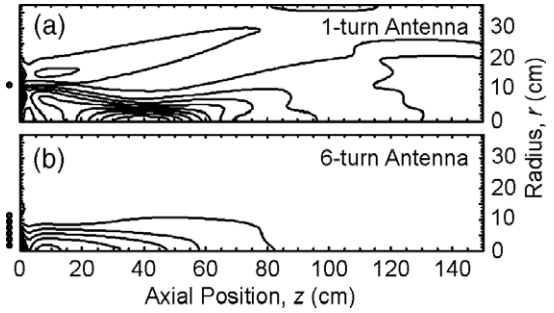


Fig. 3. Contour plots of the  $|B_z|$  field excited by (a) the single-turn and (b) the six-turn antennas. Computation parameters are as in Eq. (2).

$R=37.5$  cm and  $L=486$  cm [9], and for the following standard parameters

$$\begin{aligned} \omega/2\pi &= 7\text{MHz}, p_{Ar} = 2\text{mTorr}, T_e = 3\text{eV}, \\ n_0 &= 1 \times 10^{12} \text{cm}^{-3} \text{ and } B_0 = 50\text{G}. \end{aligned} \quad (2)$$

The fields in plasma are found to be superpositions of the bulk and surface waves. For the uniform plasma and the driving frequency  $\omega \gg \omega_{LH}$ , the lower hybrid frequency ( $\omega_{LH} \approx (\omega_{ce}\omega_{ci})^{1/2}$  where  $\omega_{ce,i}$  are the electron and ion gyro-frequencies) the wave dispersion relation takes the form

$$\frac{k_{\perp}^2 c^2}{\omega^2} = \frac{\omega_{pe}^2}{\omega \omega_{ce} (\cos \theta - \varepsilon \gamma)}, \quad (3)$$

where  $\varepsilon = \omega/\omega_{ce}$ ,  $\gamma = 1 + \nu_e/\omega$ ,  $\omega_{pe}$  and  $\nu_e$  are, respectively, the electron plasma and total collision frequencies, and  $\theta$  is the propagation angle. The wave dispersion curves are shown in Fig. 2. Long bulk waves are the helicons ( $k_{\perp} < \delta^{-1}$  where  $\delta = c/\omega_{pe}$  is the collisionless skin-size) while the short bulk waves are quasi-electrostatic (Trivelpiece-Gould) waves ( $k_{\perp} > \delta^{-1}$ ). Surface waves arise to cancel superfluous plasma polarization induced by the bulk waves near non-conducting walls. These evanescent waves are localized at the plasma–quartz window interface and are damped into plasma over short distances,  $< \delta(\omega_{ce}/\omega)^{1/2}$ , making up a few centimeters only.

To elucidate principles of wave behavior, consider first the uniform plasma. Fig. 3a shows the wave profile for a single-turn antenna of radius  $r_A = 11.5$  cm. Though helicons

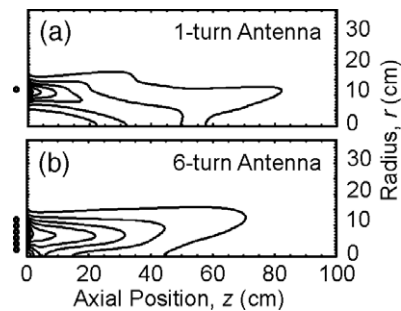


Fig. 4. Contours of the absorbed power density  $p_{abs}$  for (a) the single-turn and (b) the six-turn antennas. Computation parameters are as in Eq. (2).

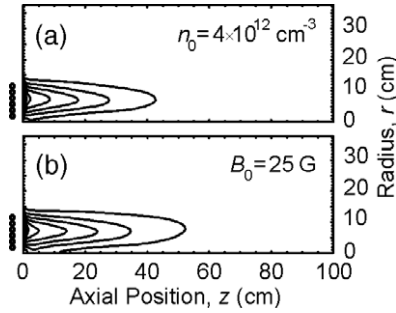


Fig. 5. Contours of  $p_{abs}$  for the six-turn antenna. Parameters are as in Eq. (2), but (a)  $n_0 = 4 \times 10^{12} \text{ cm}^{-3}$  and (b)  $B_0 = 25 \text{ G}$ .

are extremely low damped, their reflection from the back end plate is negligible owing to the large device length. Waves radiated by the antenna propagate as two narrow beams, one diverging from while the other converging to the axis. The latter beam gives rise to a strong  $B_z$  peak on the axis (a sort of the ‘magnetic focus’), at about 40 cm downstream, and becomes diverging after reflection from the axis. The second, initially diverging beam reflects from the metal wall, at  $z \approx 100 \text{ cm}$ , and then converges. Reflected beams intersect and form the interference pattern that is seen on the right of Fig. 3a.

Wave patterns alter considerably for a multi-turn antenna. As seen from Fig. 3b computed for the six-turn antenna of the same radius, interference of the wave beams irradiated by different antenna rings restricts the wave area approximately to a cylinder with the antenna as a base. Although the  $B_z$  field is stronger for the six-turn antenna, the depth of its penetration into plasma is shorter, and only a weak magnetic focus arises at  $z \approx 10 \text{ cm}$ .

Distributions of the power absorption are shown in Fig. 4. For the single-turn antenna, the power deposition is mainly along the converging cone, whereas for the six-turn antenna the absorption profile is ‘hollow’, with peak at about a mean antenna radius. Increasing density and/or decreasing magnetic field give rise to shrinking the profiles closer to the antenna, as seen from Fig. 5. The same occurs with increasing gas pressure. The effect of increasing antenna size is demonstrated in Fig. 6 computed for the four-turn antenna of larger radius  $r_A = 21.5 \text{ cm}$ . The absorption profiles are again maximum at a mean antenna

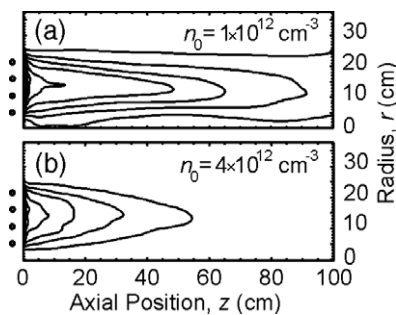


Fig. 6. Contours of  $p_{abs}$  for the four-turn antenna computed for the two values of density and the other parameters as in Eq. (2).

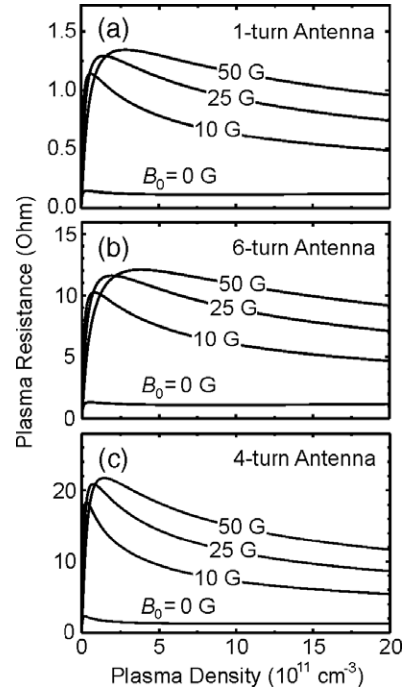


Fig. 7. Dependences of the antenna resistance on the plasma density, at various  $B_0$ , for the (a) one-turn, (b) six-turn, and (c) four-turn antennas.

radius but are more hollow than for the six-turn antenna and extend much farther from the window.

Plasma loading resistance is shown in Fig. 7. It sharply grows with density, reaches the maximum and then gradually falls. The resistance variation is smooth because the antenna works in purely radiative regime, with cavity resonances eliminated. The resistance is low at  $B_0 = 0$  but rapidly grows with magnetic field, within a few tens gauss, indicating the onset of wave propagation. The resistance magnitude increases with the number of the antenna turns and also with its radius, as a result of growing linkage flux.

### 3. Discussion and comparison with experimental results

An important effect for the large ICMP is the energy transport by helicons nearly along the magnetic lines [12].

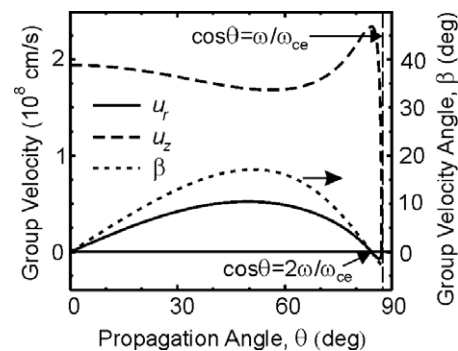


Fig. 8. The group velocity and the group velocity angle vs propagation angle. Parameters are as in Eq. (2); wave damping is neglected.

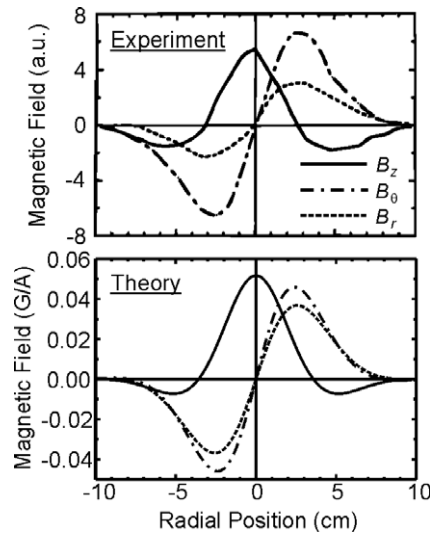


Fig. 9. Measured and computed radial profiles of the rf magnetic field.

Components of the group velocity  $u$  along and across  $B_0$  and the group velocity angle,  $\beta = \tan^{-1}(u_r/u_z)$ , are plotted as functions of the propagation angle in Fig. 8. The axial velocity is nearly constant except in a close vicinity of the resonance angle,  $\theta_{\text{res}} = \cos^{-1}(\omega/\omega_{\text{ce}})$ . The perpendicular velocity is much smaller and changes sign at an angle of helicon and TG waves merging,  $\theta_{\text{merge}} = \cos^{-1}(2\omega/\omega_{\text{ce}})$ . Being much less than  $\theta$ ,  $\beta$  has maximum,  $\beta_{\text{max}}$ , at  $\theta_{\text{max}} < \theta_{\text{merge}}$ . At  $\varepsilon \rightarrow 0$ ,  $\beta_{\text{max}} \approx 19.5^\circ$  at  $\theta_{\text{max}} \approx 54.8^\circ$  [15]; with increasing  $\varepsilon$ , both  $\beta_{\text{max}}$  and  $\theta_{\text{max}}$  decrease. For conditions of Eq. (2),  $\varepsilon \approx 0.05$  and  $\beta_{\text{max}} \approx 17.1^\circ$ . The cones of helicon waves in Fig. 3a are well within this value.

For comparison with the experiment, we made computations for the device with  $R=22.5$  cm and  $L=170$  cm excited by the four-turn antenna of radius  $r_A=9$  cm [7,8], for parameters related to the experiment:  $\omega/2\pi=7$  MHz,  $p_{\text{Ar}}=27$  mTorr,  $T_e=3$  eV and  $B_0=72$  G. As the measured plasma profile was quite uniform axially, only radial nonuniformity was considered:  $n(r)=n_0 \exp(-r^2/r_p^2)$  with  $n_0=8 \times 10^{12}$  cm $^{-3}$  and the effective plasma radius  $r_p=16$  cm. Comparison of computed and measured field profiles (Fig. 9) shows that theory correctly predicts the radial dimensions but gives some disproportion between the field amplitudes. As the uniform plasma approximation yields much wider radial profiles, focusing effect of the radial plasma nonuniformity is found to be considerable.

#### 4. Conclusions

The power in the large ICMP is deposited mainly by the helicon waves carrying the energy approximately along the

magnetic field. The surface waves excited in a narrow near-antenna region are of minor importance. Profiles of the rf fields and power absorption are strongly nonuniform; they shrink closer to the antenna with increasing density, decreasing magnetic field, and increasing pressure; i.e., behave according to the helicon wave damping.

The fields and absorption profiles depend strongly on the antenna design, as a result of interference of the waves irradiated by different antenna turns. The multi-turn antenna is similar to the phased array: it can form a directional radiation pattern and thus control the power deposition in plasma. This allows one, in principle, to optimize plasma production, but specific ways for doing this may become clear with use of more complete model that includes ionization and transport effects.

#### Acknowledgements

Continuous encouragement of Prof. Y. Kawai is greatly appreciated. This work was partly supported by the State Fund for Basic Research, Ministry of Education and Science of Ukraine under contract F7/253-2001.

#### References

- [1] R.W. Boswell, F.F. Chen, IEEE Trans. Plasma Sci. 25 (1997) 1229.
- [2] F.F. Chen, R.W. Boswell, IEEE Trans. Plasma Sci. 25 (1997) 1245.
- [3] D.B. Hayden, D.R. Juliano, M.N. Neumann, M.C. Allain, D.N. Ruzic, Surf. Coat. Technol. 120–121 (1999) 401.
- [4] K. Sasaki, H. Kokubu, D. Hayashi, K. Kadota, Thin Solid Films 386 (2001) 243.
- [5] W.T. Li, D.A.P. Bulla, C. Charles, R. Boswell, J. Love, B. Luther-Davies, Thin Solid Films 419 (2002) 82.
- [6] J.E. Stevens, M.J. Sowa, J.L. Cecchi, J. Vac. Sci. Technol. 13 (1995) 2476.
- [7] S. Shinohara, S. Takechi, Y. Kawai, Jpn. J. Appl. Phys. 35 (1996) 4503.
- [8] S. Shinohara, S. Takechi, N. Kaneda, Y. Kawai, Plasma Phys. Control. Fusion 39 (1997) 1479.
- [9] S. Shinohara, T. Tanikawa, Rev. Sci. Instrum. 75 (2004) 1941.
- [10] A. Fukuyama, Y. Ichida, in: H. Sugai, T. Hayashi (Eds.), Proc. 1996 Int. Conf. on Plasma Phys., vol. 2, Japan Soc. Plasma Sci. Nucl. Fusion Res., Nagoya, 1997, p. 1342.
- [11] S. Takechi, S. Shinohara, A. Fukuyama, Jpn. J. Appl. Phys. 38 (1999) 3716.
- [12] S. Shinohara, A. Fujii, Phys. Plasmas 8 (2001) 3018.
- [13] S.S. Kim, C.S. Chang, N.S. Yoon, K.W. Whang, Phys. Plasmas 6 (1999) 2926.
- [14] R.L. Kinder, M.J. Kushner, J. Vac. Sci. Technol., A, Vac. Surf. Films 19 (2001) 76.
- [15] D.G. Swanson, Plasma Waves, 2nd edition, IoP Publishing, Bristol, 2003, p. 62.